Geosciences Journal (2026) 30:650–662
https://doi.org/10.1007/s12303-026-00111-1

ARTICLE

Groundwater potential mapping using a frequency ratio-LSTM hybrid model in the Andijan Region, Uzbekistan

Sooyeon Han[1] · Liadira Kusuma Widya[2] · Woojin Lee[3] · Kadirhodjaev Azam[4] · Bimurzaev Gany[5]

Received: 16 March 2026 / Revised: 3 April 2026 / Accepted: 12 April 2026 / Published online: 11 June 2026

Abstract
This study develops a high-resolution groundwater potential map for the Andijan Region in the eastern Fergana Valley, Uzbekistan, by integrating the probabilistic frequency ratio (FR) method with a long short-term memory (LSTM) neural network. Eleven hydrogeomorphic, lithological, and land-surface variables—Channel Network Base Level, Closed Depressions, Cross-Sectional Curvature, DEM, Downslope Curvature, LS factor, Topographic Wetness Index, Valley Depth, Geology, Soil, and Land Cover—were derived from 12.5 m ALOS PALSAR topographic data, Sentinel imagery, and national geodatabases. FR analysis quantified the contribution of each factor to observed well yields, generating factor-specific weights and using gridded predictors as inputs to the LSTM to capture nonlinear spatial interactions. Validation against an independent dataset comprising 61 surveyed production wells showed an improvement in the area under the receiver operating characteristic curve from 75.60% for the FR model to 77.54% for the FR-LSTM ensemble, demonstrating an incremental but consistent benefit of the hybrid modeling approach. High-potential zones (> 0.8 probability) are spatially associated with Quaternary alluvial fans and the Kara Darya floodplain, where thick and highly permeable sediments, together with gentle slope gradients, favor groundwater recharge, whereas uplifted Paleozoic terrains typically exhibit low groundwater potential (< 0.2). Cross-validation indicates that 74% of high-yield wells lie within the two highest groundwater potential classes. A reproducible FR-LSTM workflow provides actionable guidance for well siting, groundwater abstraction management, and integrated water resources planning in semi-arid and data-limited basins and is readily transferable to analogous hydrogeological settings.

Keywords Groundwater potential · Frequency ratio · LSTM · Andijan · Uzbekistan

1 Introduction

A groundwater potential map (GPM) is a scientifically derived cartographic product that delineates spatial variations in the probability and likelihood of groundwater occurrence within a defined region. By classifying areas according to relative groundwater potential, a GPM provides a rational basis for prioritizing groundwater exploration and development activities, thereby reducing unnecessary drilling efforts and associated costs. Focusing development on zones with high groundwater potential is advantageous from both economic and environmental perspectives, particularly in regions where groundwater serves as a critical resource for agricultural, industrial, and domestic water supply.

In addition to supporting efficient resource development, GPMs play an increasingly important role in groundwater protection and sustainable management. Because remediation of contaminated groundwater is technically

Editorial responsibility: Saro Lee

✉ Bimurzaev Gany
gany82@mail.ru

1 Geoscience Data Research Department, Korea Institute of Geoscience and Mineral Resources, Daejeon, Republic of Korea

2 Department of Science Education, Kangwon National University, Chuncheon, Republic of Korea

3 College of AI Convergence, Dongguk University, Seoul, Republic of Korea

4 University of Geological Sciences, Tashkent, Republic of Uzbekistan

5 State Establishment Institute of Hydrogeology and Engineering Geology, Tashkent, Republic of Uzbekistan

challenging, economically costly, and often infeasible, proactive groundwater management is essential. A GPM facilitates the integrated assessment of groundwater flow pathways in relation to surrounding land-use patterns and abstraction points, thereby enabling early identification of potential contamination sources. Consequently, GPMs contribute directly to protecting drinking water quality and safeguarding public health. GPMs also provide fundamental spatial information for national and local authorities in the formulation of groundwater management plans and broader integrated water-resources strategies. Their application supports the integration of surface-water and groundwater management policies, thereby helping to avoid redundant investments and unsustainable or indiscriminate groundwater abstraction practices. In this regard, GPMs represent a key scientific and practical tool for the sustainable stewardship of groundwater resources at both regional and national scales as they improve long-term resource viability and reduce environmental and social conflicts.

Against this background, the primary objective of this study is to develop and validate a GPM for the Andijan (Uzbek: Andijon) Region of Uzbekistan using a machine-learning-based modeling approach. To achieve this objective, comprehensive and high-resolution spatial datasets related to groundwater occurrence, geology, topography, soil characteristics, and land cover were systematically compiled for the study area. Topographic data were subjected to detailed geomorphological and hydrological analyses to derive a robust set of explanatory variables that are directly relevant to groundwater occurrence and spatial distribution. The frequency ratio (FR) method was then employed to quantitatively assess the relationships between observed groundwater abstraction data and candidate conditioning factors, thereby allowing the most influential variables to be identified. These selected factors were subsequently integrated into a hybrid modeling framework that combines the FR approach with a long short-term memory (LSTM) neural network to produce the GPM. The resulting map was quantitatively evaluated using the area under the receiver operating characteristic curve (ROC-AUC), ensuring an objective assessment of predictive skill.

Numerous studies have applied probabilistic models for groundwater potential mapping. Razandi et al. (2015) demonstrated GIS-based groundwater potential mapping using a multi-criteria approach that combines FR, certainty factor (CF), and analytic hierarchy process (AHP) models. Falah et al. (2017) tested a generalized additive model and compared its performance with three GIS-based bivariate statistical models: FR, statistical index (SI), and weight of evidence. Hou et al. (2018) conducted a comparative analysis of SI, the index of entropy, and CF models for groundwater spring potential mapping. Paul et al. (2020) employed a GIS-based multi-criteria evaluation framework using weighted thematic layers to delineate spatial groundwater potential zones. Lee and Mahdi (2021) applied the FR model at the national scale of South Korea to generate a GPM. Oh et al. (2011) applied probabilistic methods to map regional groundwater potential in the Pohang City area of Korea. Lee (2025) produced a GPM for the Cheongju area using probabilistic methods, and Lee and Mahdi (2021) mapped groundwater productivity across the entirety of South Korea using a probabilistic modeling approach. Baek et al. (2021) further extended national-scale mapping efforts by applying the DRASTIC model to assess groundwater pollution vulnerability across South Korea. Remote sensing data and techniques have also been reviewed as foundational inputs for such mapping efforts (Lee, 2017).

Machine-learning-based approaches have also been widely adopted. Al-Abadi and Shahid (2016) utilized a GIS-integrated random forest model using known flowing-well locations and multiple spatial predictors. Rahmati et al. (2016) compared random forest and maximum entropy models using well-yield data in a semi-arid region. Naghibi et al. (2017, 2019) assessed data mining and ensemble approaches for groundwater potential mapping. Golkarian et al. (2018) validated decision tree-based and regression models, whereas Miraki et al. (2019) proposed a random subspace-random forest ensemble. Rizeei et al. (2019) proposed an ensemble multi-adoptive boosting logistic regression technique for groundwater aquifer potential modeling. Subsequent studies have compared or integrated advanced machine-learning algorithms, including support vector machines, boosting methods, deep neural networks, convolutional neural network-LSTM hybrids, and ensemble frameworks across diverse hydrogeological settings (Al-Fugara et al., 2020; Hakim et al., 2022; Kamali-Maskooni et al., 2020; Morgan et al., 2023; Naghibi et al., 2020; Panahi et al., 2020; Rasool et al., 2022; Roy et al., 2022).

Several studies have combined statistical and machine-learning models. Chen et al. (2018) introduced an ensemble model that combines the weight of evidence with machine learning. Kim et al. (2018) integrated the FR and evidential belief function approaches with an artificial neural network. Lee et al. (2018) applied artificial neural network and support vector machine (SVM) models within a GIS framework. Arabameri et al. (2019) compared bivariate, multivariate, machine-learning, and multi-criteria decision-making techniques; whereas Hasanuzzaman et al. (2022) evaluated AHP, FR, and machine-learning classifiers, reporting the superior performance of the random forest algorithm. Arabameri et al. (2021) further applied novel GIS-based machine-learning ensemble techniques for modeling groundwater potential.

In addition to the above references, numerous studies have investigated groundwater potential mapping using GIS and machine-learning techniques (Lee & Rezaie, 2020). Although numerous studies worldwide have generated GPMs, this study is the first to apply an FR-LSTM hybrid model to the Andijan Region of Uzbekistan, thereby providing novel, data-driven insights into regional groundwater prospectivity.

2 Study area

The Andijan Region is one of the provinces of the Republic of Uzbekistan, located in the eastern part of the Fergana Valley (Fig. 1). The Andijan Region borders the Osh Region of the Kyrgyz Republic to the north, east, and south, and borders the Namangan Region to the northwest and the Fergana Region to the southwest.

The Andijan Region extends approximately 150 km from west to east and between 35 and 75 km from north to south. The western part of the region is characterized by a plain formed by the Karadarya terraces, consisting of rocky, sandy, and fine-sand areas. The Maylisuv, Akbura, and Karadarya rivers flow through the region, originating from the Turkestan–Alay Mountains in the south and the Chatkal–Kurama ranges in the north, along with several smaller streams.

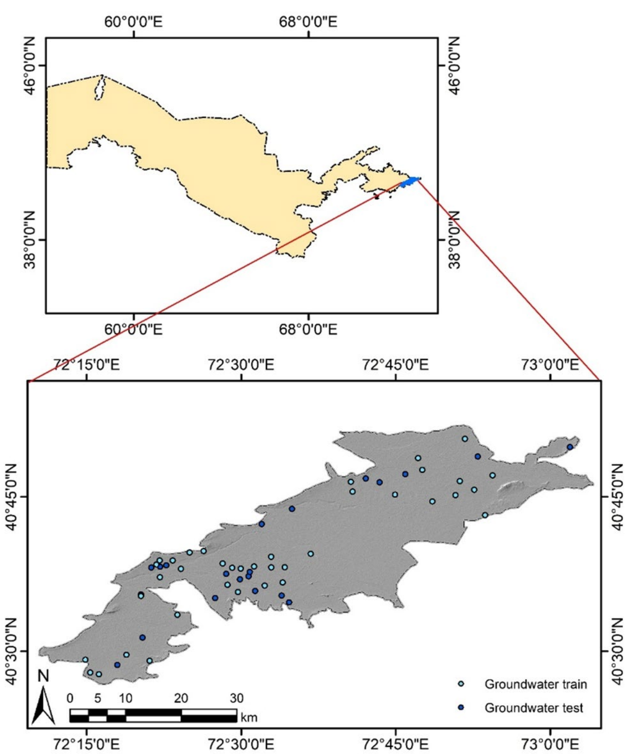

Fig. 1 Map of the study area

Geologically, the Andijan Region is situated within the eastern sector of the Fergana Valley, which represents a major intermontane tectonic depression formed in association with the Cenozoic evolution of the Tien Shan orogenic system (Brunet et al., 2017; Dobretsov et al., 1996). The valley is underlain by a Paleozoic crystalline basement overlain by thick Mesozoic–Cenozoic sedimentary successions, reflecting long-term subsidence and basin-infilling processes controlled by regional compressional tectonics and fault activity (Clarke, 1984; Nesmeyanov et al., 2021). Within the Andijan area, the surface and near-surface geology is dominated by Neogene and Quaternary deposits, including silts, clays, sands, sandstones, gravels, and conglomerates, which are extensively distributed across the plains, river terraces, and low hills of the region (Clarke, 1984; Nesmeyanov et al., 2021). Quaternary alluvial and loess deposits are particularly extensive and generally unconsolidated, making them highly sensitive to erosion, groundwater-level fluctuations, and geotechnical instability under both natural and anthropogenic loading conditions (Nesmeyanov et al., 2021; Zhang et al., 2020).

The central part of the valley is bounded by hills dissected by channels of ephemeral streams. These hills are typically composed of layers of sandstone, conglomerate, and gravel interspersed with sandstone aggregates and sandstone strata. In recent years, the slopes and previously unoccupied areas of these hills have been increasingly converted to irrigated agricultural land. The absolute elevations of the hills range from approximately 600 m to about 950–1,000 m above mean sea level. The foothill zones are separated from the adjacent mountain ranges by intervening foothill depressions, which constitute the most intensively developed and densely populated areas within the region.

Groundwater conditions are closely linked to natural factors, including air temperature, precipitation, and river discharge. The Andijan Region has a continental arid climate characterized by hot summers and moderately cold winters. The climate of Central Asia, including the Fergana Valley, is influenced by periodic intrusions of cold Arctic and warm tropical air masses, resulting in pronounced seasonal variability, particularly autumn–winter and spring. These processes contribute to winter snow accumulation in mountainous areas, thereby sustaining river discharge.

Between 2001 and 2020, the average annual air temperatures were consistently positive, ranging from 14.8 °C in 2001 to 15.2 °C in 2020. The highest temperatures occurred from June to September, with July 2019 reaching 38.7 °C, whereas minimum temperatures were recorded from November to March, with February 2014 dropping to −3.4 °C.

The Andijan Region receives relatively low and seasonally irregular precipitation, with amounts increasing toward the southeast and south. At the Andijan weather station, the average annual precipitation during 2001–2020 was 232.0 mm, with most rainfall occurring from December to March. Consequently, the moisture deficit is lowest in winter and highest in summer. Maximum annual precipitation was 292.1 mm in 2016, whereas minimum precipitation was 144.2 mm in 2013. The highest average monthly precipitation occurred in March (32.6 mm), whereas the lowest occurred in September (3.7 mm).

The research area has a well-developed hydrographic network. Major rivers include the Karadarya, Maylisuv, and Tentaksoy rivers. Numerous canals play a crucial role in regional irrigation, including the Great Fergana, Great Andijan, South Fergana, Savay, Baliqchi, Ulug'nor, Andijansoy, and Shahrixonsoy canal systems. The Andijan Reservoir on the Karadarya River regulates water distribution throughout the year. Canal discharge ranges from approximately 35 m^3/s in the Ulug'nor Canal to 200 m^3/s in the Great Fergana and Great Andijan Canals.

Water levels increase mainly during spring and summer, coinciding with irrigation activities, and decrease after the irrigation season ends. Water is primarily used for agricultural irrigation. In addition, an extensive collector and drainage system operates in the region, with a total length of 3,258.89 km. These systems drain groundwater from irrigated and residential areas, thereby preventing flooding, reducing salinity, and improving land reclamation conditions.

3 Data

GPM is a scientifically derived spatial product that integrates topographic, geological, hydrological, and environmental datasets to delineate areas with varying likelihoods of groundwater occurrence. The development of a reliable GPM requires the systematic compilation and integration of multiple datasets representing both surface and subsurface hydrogeological conditions (Han & Han, 2022). From available datasets, factors exhibiting FR correlation ≥ 0.5 were selected for groundwater potential modeling, including geomorphological factors derived from 12.5 m ALOS PALSAR DEM and thematic layers (geology from Uzbekistan Ministry of Geology, soil from FAO HWSD, land cover from Sentinel-2 Level-2 A 10 m). The study utilized 61 surveyed production wells (label = 1) complemented by 61 zero-value locations (value = 0) randomly selected from very low groundwater potential zones, ensuring a balanced 1:1 ratio. The 122-point dataset was partitioned 70:30 as train and test points using constrained random sampling with inter-point distance to mitigate spatial autocorrelation. The 11 variables selected through FR analysis, including channel network base level, closed depressions, cross-sectional curvature, DEM, downslope curvature, slope length and steepness factor (LS factor), topographic wetness index (TWI), valley depth, geology, soil and land cover, exhibited FR correlation ≥ 0.5 and were used as input factors (Table 1; Fig. 2). The following sections describe each factor and its relevance to groundwater occurrence.

The channel network base level represents the lowest elevation of a drainage system, effectively defining the limiting level below which stream incision cannot occur. This base level controls the outlet conditions for groundwater flow; groundwater tables generally slope toward the channel base level, and groundwater is discharged as springs or baseflow upon reaching this elevation. A lower base level can induce groundwater drawdown by steepening hydraulic gradients and accelerating groundwater flow toward stream channels, whereas a higher or closed base level (e.g., an inland basin) may promote groundwater accumulation, resulting in a progressive rise in the water table until discharge occurs at the base-level elevation.

Closed depressions are enclosed topographic lows that lack a surface drainage outlet; consequently, water accumulating within these features can escape only through

Table 1 Groundwater potential-affecting variables used in the study

Variable type	Variable name	Data Source
Geomorphological Factor	Channel Network Base Level	ALOS PALSAR RTC DEM (ASF DAAC, 12.5 m)
	Closed Depressions	
	Cross-Sectional Curvature	
	DEM	
	Downslope Curvature	
	Slope Length and Steepness Factor (LS factor)	
	Topographic Wetness Index (TWI)	
	Valley Depth	
Geology	Geology	Ministry of Mining Industry and Geology of the Republic of Uzbekistan
Soil	Soil	FAO Harmonized World Soil Database
Land Cover	Land Cover	Sentinel-2 Level-2 A (Copernicus Hub, 10 m)

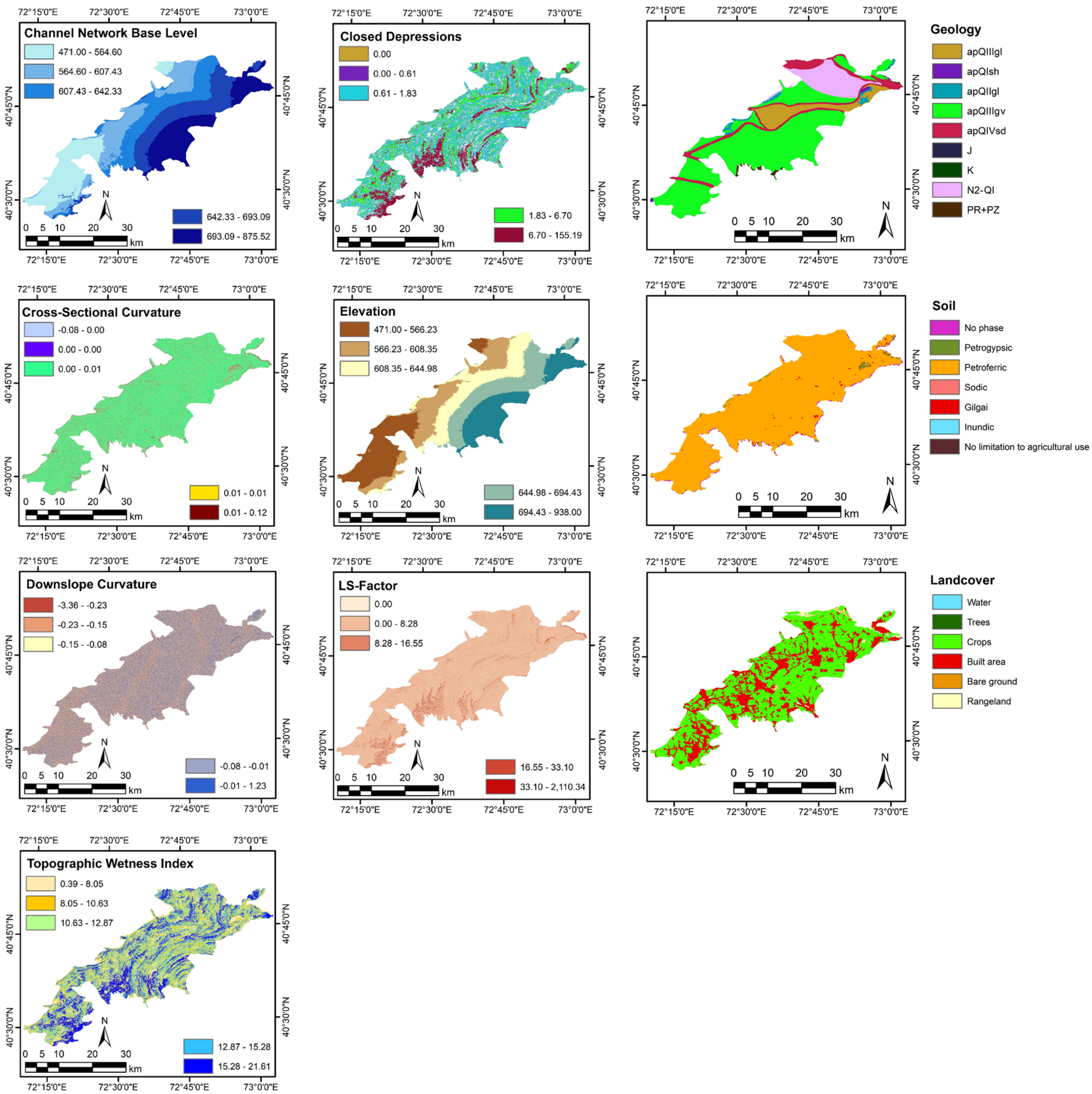

Fig. 2 Input factors for groundwater potential mapping in Andijan Region, Uzbekistan

evaporation or infiltration into the subsurface. These features function as natural traps for surface runoff and frequently serve as focused recharge zones; water that pools within closed depressions has increased residence time for infiltration, resulting in enhanced and spatially concentrated groundwater recharge. If the underlying soil or bedrock is sufficiently permeable, closed depressions (e.g., karst sinkholes or playas) can efficiently channel surface water into underlying aquifers, thereby increasing localized groundwater storage capacity.

Cross-sectional curvature refers to the curvature of the land surface measured perpendicular to the downslope direction and is conceptually equivalent to the curvature of contour lines. It indicates whether a hillside exhibits lateral convexity or concavity when viewed across the slope. Cross-sectional (plan) curvature exerts control over the convergence or divergence of surface water flow across hill slopes. Concave cross-sectional curvature concentrates surface runoff into topographic hollows, thereby increasing soil moisture availability and infiltration rates, which may enhance groundwater recharge potential. Conversely, convex cross-sectional curvature disperses water laterally, promoting rapid runoff and reduced localized infiltration, thereby diminishing recharge potential on convex slope areas.

A DEM is a gridded representation of ground-surface elevations. It provides the fundamental topographic data from which key terrain attributes—such as slope, curvature, and hydrological flow paths—are systematically derived. Terrain elevation strongly governs groundwater flow patterns; water in unconfined aquifers generally flows from higher to lower elevations under the influence of gravitational forces. Thus, DEM-based analyses can be used to estimate groundwater flow directions and to identify recharge and discharge areas. Elevated areas in the DEM often correspond to recharge zones where water percolates downward, whereas low-lying areas commonly coincide with discharge zones where the water table intersects the land surface, thereby supporting springs, wetlands, or sustained stream baseflow (Lee & Kim, 2020, 2021).

Downslope curvature (also referred to as profile or longitudinal curvature) is the curvature of the terrain measured in the direction of steepest slope. It describes whether a slope exhibits convexity or concavity when viewed from the side. Downslope curvature affects the acceleration and deceleration of surface runoff, which in turn influences opportunities for water infiltration. Convex slope profiles shed water rapidly from upper slope segments, often resulting in reduced infiltration. In contrast, concave slope profiles promote water accumulation near the lower slope, thereby enhancing moisture retention and groundwater recharge near the footslope or valley floor. In essence, convex downslope curvature is associated with lower water retention, whereas concave curvature is associated with higher water retention and increased recharge potential at slope bases.

LS factor is a dimensionless index representing the combined effect of slope length and slope steepness on erosion and runoff generation. Although primarily an erosion metric, it is relevant to hydrological processes because it reflects slope-controlled surface-water dynamics. High LS values indicate rapid downslope flow and reduced infiltration capacity, whereas low LS values imply slower runoff and increased infiltration, thereby favoring groundwater recharge.

TWI is a steady-state index that integrates upslope contributing area and local slope. TWI characterizes the tendency of a given landscape position to accumulate water. High TWI values are typically associated with valley bottoms or concave areas where water accumulation and infiltration are enhanced, thereby increasing groundwater recharge potential. Low TWI values occur on steep or well-drained terrain, where rapid surface runoff limits groundwater recharge. Owing to its strong relationship with soil moisture distribution and subsurface flow processes, TWI is widely used as a conditioning factor in groundwater potential mapping.

Valley depth measures the vertical difference between valley floors and the surrounding terrain, reflecting the degree of valley incision. Deep valleys commonly act as groundwater discharge zones, where the water table intersects the land surface and supplies streams or springs through baseflow. Shallow valleys typically exhibit more diffuse groundwater discharge patterns. Therefore, valley depth mapping helps distinguish groundwater recharge areas from discharge-dominated zones.

Geology encompasses the rock and sediment types, their structural characteristics, and stratigraphic relationships beneath the surface. Key geological units in the Fergana Valley of Uzbekistan include: apQIIIgl (Upper Pleistocene gravelly alluvium: coarse piedmont gravels from Tien Shan erosion), apQIsh (Upper Pleistocene lithologic alluvium/shale), apQIIgl (Lower Pleistocene sandy loam/glacial gravel), apQIIIgv (Upper Pleistocene gravelly volcanics), apQIVsd (Holocene sandy deposits: modern river alluvium), J (Jurassic sedimentary rocks), K (Cretaceous carbonate/sandstone), N2–Q1 (Neogene–Quaternary volcanic tuffs: Andijan Formation equivalent), and PR + PZ (Paleozoic metamorphic granite basement). These units determine aquifer distribution, porosity, permeability, recharge potential, and subsurface flow paths in Fergana's intermontane basin. Unconsolidated Quaternary gravels and sands (apQIIIgl, apQIVsd) form high-transmissivity aquifers with excellent recharge from mountain rivers, while Paleozoic basement (PR + PZ) and volcanic tuffs (N2–Q1) act as low-permeability confining layers or fractured bedrock aquifers.

Soil is the unconsolidated upper layer of the Earth's surface composed of mineral particles and organic matter. Properties such as texture, structure, and permeability strongly control water movement and subsurface storage. Coarse-textured or well-structured soils allow rapid percolation and promote groundwater recharge, whereas fine-textured or compacted soils impede infiltration and increase surface runoff. Soil depth and moisture-holding capacity further influence subsurface water storage and groundwater replenishment rates.

Land cover refers to the physical cover of the land surface, including forests, grasslands, agricultural areas, urban surfaces, and water bodies. It influences vegetation density, soil exposure, and the degree of surface imperviousness. Land cover controls infiltration and groundwater recharge by regulating the partitioning of rainfall between subsurface infiltration and surface runoff. Vegetated and permeable land covers promote higher infiltration rates, whereas impermeable or sparsely vegetated surfaces increase runoff and reduce groundwater recharge. Changes in land cover, therefore, directly affect groundwater systems, as conversion to impervious surfaces diminishes soil infiltration capacity and groundwater replenishment rates.

4 Models

The FR method is a simple yet fundamental probabilistic model used to generate vulnerability or potential maps. The frequency ratio method quantifies the spatial relationship between event occurrences and their associated conditioning factors. Among the input data used to compile vulnerability or potential maps, nominal variables are grouped by category, whereas numerical variables are classified into an appropriate number of classes (e.g., five or ten); the frequency ratio for each input type or class represents the proportion of event occurrences. These frequency ratios are applied within a GIS framework to determine spatial correlations between various input datasets—such as topography, geology, soils, forest cover, and land cover—and events such as landslides, floods, ground subsidence, groundwater resources, and mineral deposits during the generation of vulnerability or potential maps. The correlations derived using frequency ratios, therefore, serve as objective criteria for selecting relevant input variables.

The frequency ratio for an event is calculated by dividing the occurrence-area (or count) proportion $PC\,(P)$ of each category or class by the corresponding total-area proportion, $PC\,(0)$ of that category or class. Thus, the frequency ratio coefficient (FRC) for each factor type or class is mathematically expressed as follows:

$$FRC = \frac{PC\,(P)}{PC\,(0)}. \tag{1}$$

Frequency ratios are used to quantify and evaluate the strength of correlation between each factor type or class and an event. Higher frequency ratio values indicate a stronger association with the event, whereas lower values indicate a weaker association. By computing the frequency ratios for all input variables and summing them spatially (Eq. 2), a vulnerability or potential map for a specific event can be obtained. In the study, the specific event considered is groundwater potential.

$$EI = \Sigma\, FR, \tag{2}$$

where EI denotes the event index, and $\Sigma\, FR$ represents the frequency ratio associated with each conditioning factor. LSTM networks are a type of recurrent neural network architecture introduced by Hochreiter and Schmidhuber (1997) to overcome the vanishing gradient problem that hampers the training of conventional RNNs. The core innovation of LSTM lies in the inclusion of gating mechanisms that regulate the flow of information into and out of a memory cell, enabling the network to maintain long-term dependencies without the gradient signal decaying over time (Mienye et al., 2024).

An LSTM cell contains an internal cell state (memory) and three gates that modulate the cell state and the hidden output at each time step: an input gate, a forget gate, and an output gate. The input gate controls how much new information is written to the cell state; the forget gate regulates the retention of the previous cell state; and the output gate controls the exposure of the cell state to the output (hidden state). Each gate's value is produced by a sigmoid activation function (range, 0–1) applied to a linear combination of the current input and the previous hidden state. The cell state is subsequently updated at each time step. This gating-and-addition structure creates an effective "constant error carousel" that preserves long-term information: the self-recurrent connection of the cell, with a fixed weight of 1, enables gradients to propagate over many time steps without vanishing. By learning when to retain and when to discard information, LSTMs mitigate vanishing gradients and capture long-range temporal patterns more effectively than traditional RNNs. Consequently, LSTMs are widely used in sequence-modeling applications such as natural language processing (e.g., language modeling and machine translation), speech recognition, and time-series forecasting, where long-term context is crucial (Gers et al., 1999; Mienye et al., 2024).

In this study, the FR-LSTM hybrid model integrated FR-derived factor weights as input features to a bidirectional LSTM network (TensorFlow/Keras) to explore potential nonlinear spatial dependency capture for groundwater potential mapping in the Andijan Region. Spatial raster predictors were restructured into 1D sequences using 11×11 pixel moving windows (121 pixels × 11 variables = 1,331 features per sequence), with row-wise flattening converting 2D spatial patterns into temporal-like sequences for LSTM processing. The architecture comprised a BiLSTM layer with 100 units (input shape = (1, 1331)), followed by a Dropout layer (rate = 0.5), a Dense layer with 10 units and ReLU activation, and a final Dense layer with one unit generating groundwater potential indices (0–1). The model was compiled using the Adam optimizer (learning rate = 0.0023) with mean squared error (MSE) loss, a batch size of 64, and a maximum of 200 epochs. Training included EarlyStopping (patience = 20), ModelCheckpoint, and TensorBoard logging.

The model's performance was evaluated using ROC analysis, an approach commonly applied in geohazard modeling studies (Fawcett, 2006). The ROC analysis is based on a curve representing sensitivity plotted along the ordinate axis versus specificity plotted along the abscissa. Sensitivity refers to the proportion of groundwater occurrence pixels correctly identified, whereas specificity refers to the proportion of non-occurrence pixels correctly identified, as derived from the confusion matrix (Fawcett, 2006). The area under the ROC curve (AUC) is used to assess the model's predictive performance by evaluating its ability to distinguish between the occurrence and non-occurrence of events. Specifically, an AUC value of 1 indicates perfect agreement between observed and modeled data, whereas a value of 0.5 indicates no predictive skill, corresponding to a random fit (Choubin et al., 2019; Fawcett, 2006).

5 Results

The relationships between groundwater occurrence and individual conditioning factors were systematically evaluated using the FR method. The resulting spatial patterns and FR distributions are illustrated in Fig. 3. The FR results for each conditioning factor are summarized below. For the channel network base level, FR values peak at class 2 (approximately 1.98) and then decrease sharply to 0.08 by class 5. This pattern indicates that groundwater potential is highest near the local base level and declines rapidly with increasing elevation; overall, higher class values correspond to progressively lower groundwater potential. For closed depressions, FR values increase monotonically from 0 at class 1 to 1.59 at class 5, suggesting that deeper or more developed depressions enhance runoff concentration and groundwater recharge, thereby increasing groundwater potential with increasing class level. For cross-sectional curvature, concave slopes (class 1; FR $\approx$ 1.33) exhibit substantially higher groundwater potential than convex slopes (class 5; FR $\approx$ 0.70). The FR values decrease consistently as curvature transitions from concave to convex forms. Regarding DEM (elevation), the lowest elevation class (class 1) shows the highest FR value (approximately 1.95), whereas FR values drop below 0.1 in the highest elevation class. This trend indicates a rapid decrease in groundwater potential with increasing terrain elevation. For downslope curvature, FR values decrease from 1.31 for concave profiles (class 1) to 0.72 for convex profiles (class 5). Concave slope profiles favor groundwater recharge by concentrating subsurface flow, whereas convex profiles promote surface runoff and reduce infiltration. The LS factor (slope length-steepness) exhibits a clear increasing trend, with FR values rising from 0.63 for gentle and short slopes to 2.13 for steep and long slopes. This pattern suggests that extended and steep slopes effectively channel surface runoff toward downslope areas, indirectly enhancing groundwater potential in footslope or valley zones. For the topographic wetness index, FR values increase from 0.68 in the lowest class to 1.31 in the highest class, indicating that wetter and flatter areas favor moisture accumulation and groundwater recharge, whereas steep and well-drained areas exhibit lower groundwater potential. For valley depth, FR values show a gradual increase from 0.96 for shallow valleys to 1.23 for deeper valleys, followed by stabilization. This trend suggests that deeply incised valleys act as major groundwater discharge zones and are associated with relatively higher groundwater potential.

For Geology, FR values range between 0 and 1.20 without a systematic trend across classes, indicating that the lithological influence on groundwater potential is unit-specific rather than ordinal in nature. Certain geological units enhance groundwater potential, whereas others restrict groundwater occurrence and storage. For soil, FR values reach a maximum at class 2 (approximately 1.01) and then decrease progressively to zero by class 5. Permeable soils in the lower classes promote infiltration, whereas fine-textured or compacted soils in higher classes inhibit groundwater recharge. For land cover, FR values vary irregularly between 0 and 1.68, indicating a weak correlation with class ranking. Vegetated or permeable land-cover types (generally presented by intermediate classes) slightly increase groundwater potential, whereas impervious or barren surfaces tend to reduce groundwater recharge potential.

Following FR and FR-LSTM hybrid model training, a groundwater potential index was assigned to each grid cell across the study area. Factor-specific class weights derived from the FR analysis were applied, and GPMs were subsequently generated within an ArcGIS environment. For visualization purposes, the continuous index values were reclassified into five groundwater potential classes—very low, low, moderate, high, and very high—based on area-based proportions of 40%, 20%, 20%, 10%, and 10%, respectively (Fig. 4). This classification follows established GPM protocols that ensure balanced representation for administrative decision-making, while maintaining $\geq$ 10% high/very high potential areas for practical groundwater management and preventing over-classification of marginal zones (Kim & Lee, 2023).

Model performance was evaluated using an independent test dataset in conjunction with ROC analysis. The ROC curves for both models are presented in Fig. 5. The FR model achieved an AUC value of 75.60%, whereas the FR-LSTM hybrid model achieved a slightly higher AUC value of 77.54%, indicating improved predictive performance for the hybrid modeling approach.

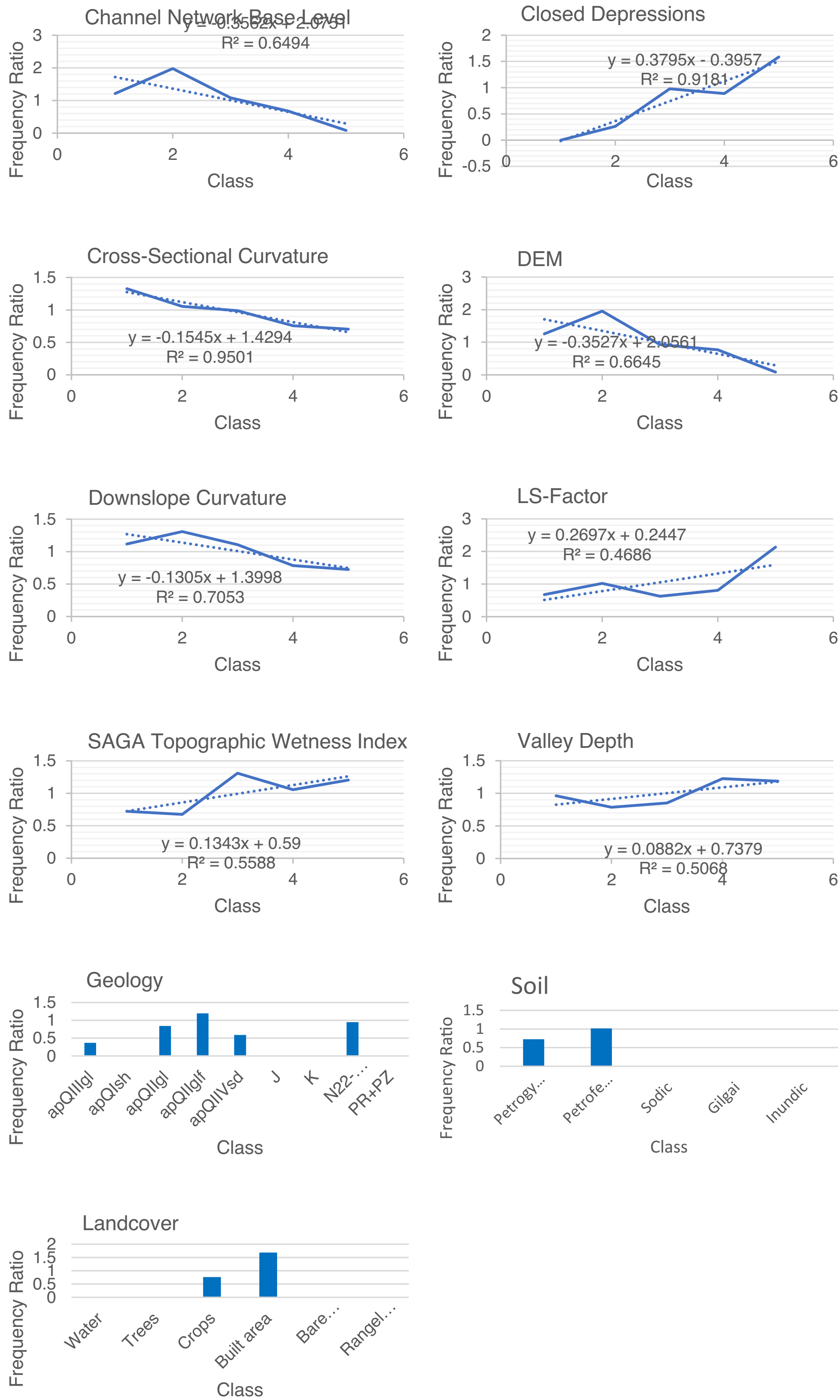

Fig. 3 Relationships between groundwater potential and conditioning factors

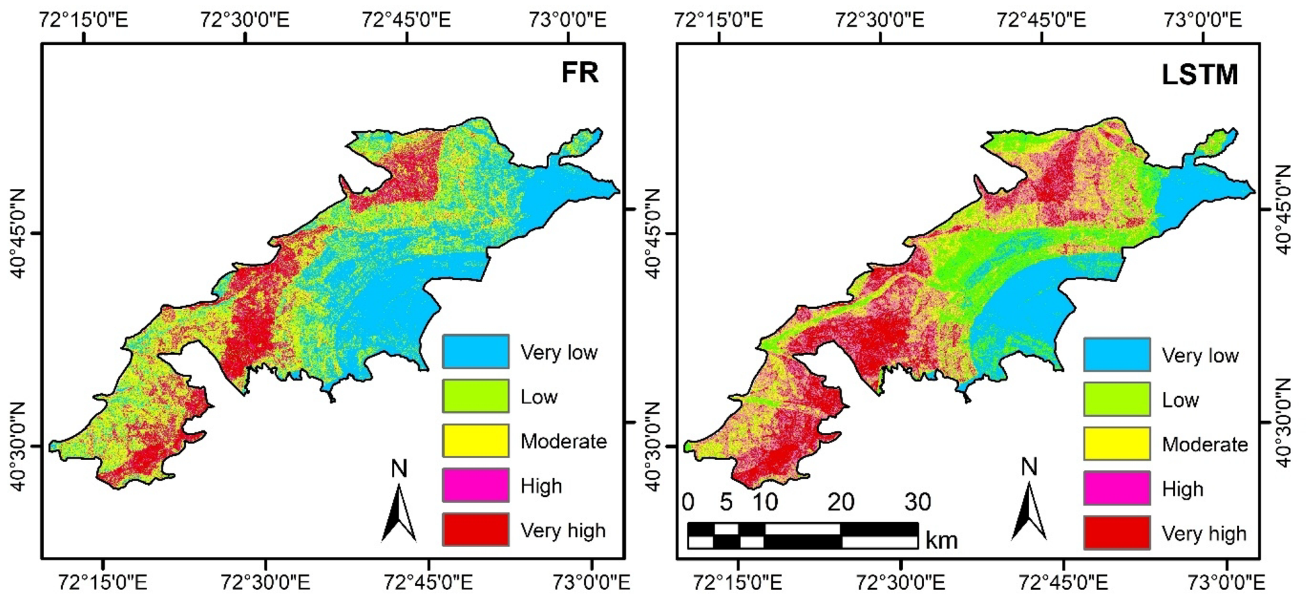

Fig. 4 Groundwater Potential maps developed using (**a**) the FR model and (**b**) the FR-LSTM Hybrid model

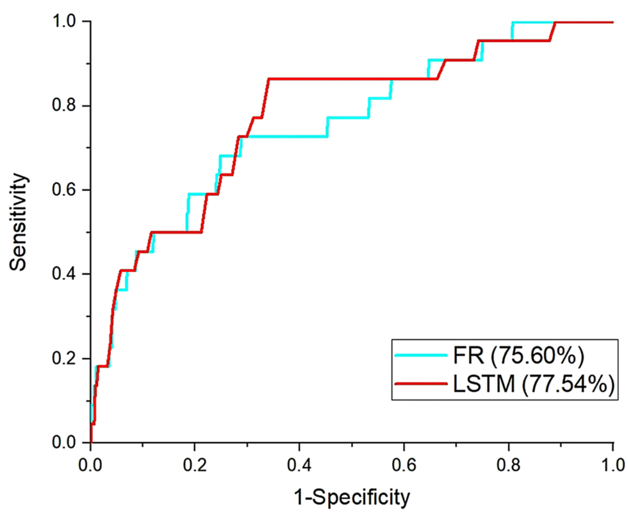

Fig. 5 ROC-AUC plots derived from the FR and FR-LSTM hybrid models

6 Conclusion and discussion

As described in Sect. 5, the FR-LSTM hybrid model achieved a marginally higher AUC (77.54%) than the standalone FR model (75.60%), and the resulting groundwater potential map was classified into five zones ranging from very low to very high potential (Fig. 4). Although the performance gain is modest, it confirms that incorporating nonlinear spatial dependency through the LSTM architecture provides an incremental but meaningful improvement over the purely probabilistic FR baseline.

GPMs provide a spatial ranking of terrain according to expected groundwater yield, enabling drilling and development activities to be strategically prioritized in high-potential zones. This targeted approach reduces exploratory drilling costs, improves well success rates, and supports the provision of reliable water supplies for agricultural, industrial, and domestic uses. At the policy level, such maps are commonly incorporated into basic groundwater plans and comprehensive water resource management strategies, where they serve as spatial evidence for integrating surface water and groundwater management within an integrated water resources management framework. Their application helps to avoid redundant investments and indiscriminate groundwater abstraction practices.

In addition, GPMs support environmental impact assessment and ecosystem protection by clearly illustrating hydraulic connections among aquifers, rivers, and associated wetland systems. This information facilitates the identification of recharge and discharge pathways and assists in the pre-selection of monitoring locations and pollution control measures. From a risk management perspective, the maps also contribute to disaster preparedness by identifying areas susceptible to groundwater drawdown, land subsidence, drought stress, or contamination, thereby enabling the proactive development of alternative supply strategies.

Integrating topographic and environmental indices into groundwater potential assessment offers several methodological and practical advantages. First, it reduces the likelihood of dry or low-yield wells by guiding exploration activities toward the most promising locations. Second, the GIS-based and quantitative nature of the approach provides objective and reproducible evidence to support holistic water resource management that considers interactions among terrain, geology, soils, and ecosystems. Third, the resulting maps highlight zones that may be particularly vulnerable to contamination or groundwater overextraction, thereby allowing planners and regulators to proactively identify and protect sensitive areas prior to major development activities or infrastructure investments.

Despite these advantages, several methodological and practical limitations should be acknowledged. The modest performance improvement of the FR-LSTM model (77.54% versus 75.60% AUC) may reflect inherent characteristics of spatial models rather than a genuine predictive gain. We did not conduct adequate statistical tests, such as DeLong's, to substantiate that the improvement was genuine rather than coincidental. LSTM is primarily intended for time series analysis rather than geographical mapping. The conversion of raster grids into sequences row-by-row was a necessary methodological compromise, which was likely suboptimal compared to convolutional neural networks that more effectively handle spatial data. The LSTM architecture involves a substantially larger number of parameters, whereas tree-based models such as Random Forest or XGBoost may yield comparable performance with considerably lower computational complexity.

GPMs inevitably simplify spatial heterogeneity, and reliance on a single modeling framework or a limited set of conditioning factors may overlook important local complexities, particularly in fractured, karstic, or fault-controlled hydrogeological settings. In addition, most GPMs represent static conditions and may fail to capture rapid temporal changes in groundwater levels, flow regimes, or water quality unless they are regularly updated. Long-term predictive uncertainty remains substantial, as climate change, land-use transitions, and emerging contaminants can alter recharge processes and aquifer dynamics in ways that are difficult to parameterize explicitly. Complex subsurface structures, legacy wells, and diffuse pollution sources further contribute to predictive uncertainty and often require dense, high-quality datasets that are rarely available in practice.

Future developments should emphasize statistical validation (DeLong test, bootstrapping), spatial-native architectures (CNN, ConvLSTM), tree-based benchmarks (XGBoost, LightGBM), and hybrid ensembles that integrate FR's interpretability with the efficacy of machine learning. Dynamic, data-intensive frameworks are likely to integrate heterogeneous datasets, including satellite imagery, LiDAR-derived topography, soil and geological properties, climatic indices, and geochemical indicators, to generate higher-resolution probabilistic outputs with explicit and quantifiable uncertainty estimates. Time-series-based approaches will enable the development of dynamic GPMs that evolve in response to seasonal recharge, groundwater abstraction patterns, and land-use change. Three- and four-dimensional visualization techniques will further enhance process understanding by representing aquifer properties, groundwater levels, and flow pathways through depth and time. In parallel, real-time data assimilation from IoT-based sensor networks—such as automated groundwater-level loggers, water-quality probes, and meteorological stations—when combined with cloud-based GIS platforms, will support near-real-time model updating and enhanced multi-agency collaboration. Hybrid ensemble frameworks that integrate water-balance models, numerical groundwater flow simulations, and data-driven approaches, underpinned by standardized data and metadata protocols, hold particular promise for improving the transferability, robustness, and long-term decision-making value of GPMs.

Acknowledgements The authors would like to acknowledge the support provided by KOICA and NRF.

Funding This research was supported by "PMC Service for the Establishment of Integrated Management System for Mineral Resources and Geological Disaster in Uzbekistan (26-5209)" funded by the KOICA and the National Research Foundation of Korea (NRF) grant funded by the Korea government (MSIT) (No. 2023R1A2C1003095).

Data availability The ALOS PALSAR DEM data used in this study are available at https://search.asf.alaska.edu/. The Sentinel imagery for land cover analysis is available at https://sentinels.copernicus.eu/.

Declarations

Competing Interests The authors declare that they have no competing interests.

References

Al-Abadi, A. M., & Shahid, S. (2016). Spatial mapping of artesian zone at Iraqi southern desert using a GIS-based random forest machine learning model. *Modeling Earth Systems and Environment*, *2*(2), 96. https://doi.org/10.1007/s40808-016-0150-6

Al-Fugara, A. K., Pourghasemi, H. R., Al-Shabeeb, A. R., Habib, M., Al-Adamat, R., Al-Amoush, H., & Collins, A. L. (2020). A comparison of machine learning models for the mapping of groundwater spring potential. *Environmental Earth Sciences*, *79*(10), 206. https://doi.org/10.1007/s12665-020-08944-1

Arabameri, A., Rezaei, K., Cerdà, A., Lombardo, L., & Rodrigo-Comino, J. (2019). GIS-based groundwater potential mapping in Shahroud Plain, Iran: A comparison among bivariate, multivariate, data mining, and multi-criteria decision-making approaches. *Science of the Total Environment*, *658*, 160–177. https://doi.org/10.1016/j.scitotenv.2018.12.115

Arabameri, A., Pal, S. C., Rezaie, F., Nalivan, O. A., Chowdhuri, I., Saha, A., Lee, S., & Moayedi, H. (2021). Modeling groundwater potential using novel GIS-based machine-learning ensemble techniques. *Journal of Hydrology: Regional Studies*, *36*, 100848. https://doi.org/10.1016/j.ejrh.2021.100848

Baek, W. K., Park, S. H., Yu, J. W., Yoon, Y. W., & Jeong, H. S. (2021). Mapping of groundwater pollution vulnerability in entire South Korea using DRASTIC model. *GEO DATA*, *3*(2), 32–38. https://doi.org/10.22761/DJ2021.3.2.005

Brunet, M. F., Korotaev, M. V., Ershov, A. V., & Nikishin, A. M. (2017). Geological evolution of Central Asian basins and the western Tien Shan Range: Integration of new results. In M. F. Brunet, T. McCann, & E. R. Sobel (Eds.), *Tectonic evolution of the Tien Shan Belt* (Vol. 427, pp. 23–52). Geological Society of London. https://doi.org/10.1144/SP427.17

Chen, W., Li, H., Hou, E., Wang, S., & Panahi, M. (2018). GIS-based groundwater potential analysis using novel ensemble weights-of-evidence with logistic regression and functional tree models. *Science of the Total Environment*, *634*, 853–867. https://doi.org/10.1016/j.scitotenv.2018.04.055

Choubin, B., Moradi, E., Golshan, M., Adamowski, J., Sajedi-Hosseini, F., & Mosavi, A. (2019). An ensemble prediction of flood susceptibility using multivariate discriminant analysis, classification and regression trees, and support vector machines. *Science of the Total Environment*, *651*, 2087–2096. https://doi.org/10.1016/j.scitotenv.2018.10.064

Clarke, J. W. (1984). *Geology and possible uranium deposits of the Fergana region of Soviet Central Asia* (Open-File Report 84–513). U.S. Geological Survey. https://pubs.usgs.gov/of/1984/0513/report.pdf

Dobretsov, N. L., Buslov, M. M., Delvaux, D., Berzin, N. A., & Ermikov, V. D. (1996). Meso- and Cenozoic tectonics of the Central Asian mountain belt: Effects of lithospheric plate interaction and mantle plumes. *International Geology Review*, *38*(5), 430–466. https://doi.org/10.1080/00206819709465345

Falah, F., Ghorbani Nejad, S., Rahmati, O., Daneshfar, M., & Zeinivand, H. (2017). Applicability of generalized additive model in groundwater potential modelling and comparison its performance by bivariate statistical methods. *Geocarto International*, *32*(10), 1069–1089. https://doi.org/10.1080/10106049.2016.1188166

Fawcett, T. (2006). An introduction to ROC analysis. *Pattern Recognition Letters*, *27*(8), 861–874. https://doi.org/10.1016/j.patrec.2005.10.010

Gers, F. A., Schmidhuber, J., & Cummins, F. (1999). Learning to forget: Continual prediction with LSTM. In *Proceedings of the 9th International Conference on Artificial Neural Networks* (ICANN '99) (pp. 850–855). https://doi.org/10.1049/cp:19991218

Golkarian, A., Naghibi, S. A., Kalantar, B., & Pradhan, B. (2018). Groundwater potential mapping using C5.0, random forest, and multivariate adaptive regression splines: A comparative study. *Environmental Monitoring and Assessment*, *190*(3), 149. https://doi.org/10.1007/s10661-018-6507-8

Hakim, W. L., Nur, A. S., Rezaie, F., Panahi, M., Lee, C. W., & Lee, S. (2022). Convolutional neural network and long short-term memory algorithms for groundwater potential mapping in Anseong, South Korea. *Journal of Hydrology: Regional Studies*, *39*, 100990. https://doi.org/10.1016/j.ejrh.2022.100990

Han, S., & Han, J. (2022). Case study on an integrated interoperable metadata model for geoscience information resources. *Geoscience Data Journal*, *9*(2), 355–370. https://doi.org/10.1002/gdj3.150

Hasanuzzaman, M., Mandal, M. H., Hasnine, M., & Shit, P. K. (2022). Groundwater potential mapping using multi-criteria decision, bivariate statistic and machine learning algorithms: Evidence from the Chota Nagpur Plateau, India. *Applied Water Science*, *12*(1), 58. https://doi.org/10.1007/s13201-022-01584-9

Hochreiter, S., & Schmidhuber, J. (1997). Long short-term memory. *Neural Computation*, *9*(8), 1735–1780. https://doi.org/10.1162/neco.1997.9.8.1735

Hou, E., Wang, J., & Chen, W. (2018). A comparative study on groundwater spring potential analysis based on statistical index, index of entropy and certainty factors models. *Geocarto International*, *33*(7), 754–769. https://doi.org/10.1080/10106049.2017.1299801

Kamali-Maskooni, E., Naghibi, S. A., Hashemi, H., & Berndtsson, R. (2020). Application of advanced machine learning algorithms to assess groundwater potential using remote sensing-derived data. *Remote Sensing*, *12*(17), 2742. https://doi.org/10.3390/rs12172742

Kim, J-C., & Lee, S. (2023). Comparative Study of Deep Neural Networks for Landslide Susceptibility Assessment: A Case Study of Pyeongchang-gun, South Korea. *Sustainability*, *16*, 245. https://doi.org/10.3390/su16010245

Kim, J. C., Jung, H. S., & Lee, S. (2018). Groundwater productivity potential mapping using frequency ratio and evidential belief function and artificial neural network models: Focus on topographic factors. *Journal of Hydroinformatics*, *20*(6), 1436–1451. https://doi.org/10.2166/hydro.2018.120

Lee, J. (2017). Review of remote sensing studies on groundwater resources. *Korean Journal of Remote Sensing*, *33*(5), 855–866. https://doi.org/10.7780/kjrs.2017.33.5.3.8

Lee, S. (2025). Groundwater potential map data of Cheongju area using probabilistic methods. *GEO DATA*, *7*(3), 160–171. https://doi.org/10.22761/GD.2025.0013

Lee, S., & Kim, M. (2020). Construction of topographic/hydrologic data using DEM and its service. *GEO DATA*, *2*(2), 36–44. https://doi.org/10.22761/DJ2020.2.2.006

Lee, S., & Kim, M. (2021). Construction of topographic/hydrologic data using DEM and its service 2. *GEO DATA*, *3*(4), 1–10. https://doi.org/10.22761/DJ2021.3.4.001

Lee, S., & Mahdi, P. (2021). Mapping of groundwater productivity in entire South Korea using probabilistic model. *Geo Data*, *3*(2), 25–31. https://doi.org/10.22761/DJ2021.3.2.004

Lee, S., & Rezaie, F. (2020). Status of groundwater potential mapping research using GIS and machine learning. *Korean Journal of Remote Sensing, 36(6–1)*, 1277–1290. https://doi.org/10.7780/kjrs.2020.36.6.1.1

Lee, S., Hong, S. M., & Jung, H. S. (2018). GIS-based groundwater potential mapping using artificial neural network and support vector machine models: The case of Boryeong city in Korea. *Geocarto International*, *33*(8), 847–861. https://doi.org/10.1080/10106049.2017.1303091

Mienye, I. D., Swart, T. G., & Obaido, G. (2024). Recurrent neural networks: A comprehensive review of architectures, variants, and applications. *Information*, *15*(9), 517. https://doi.org/10.3390/info15090517

Miraki, S., Zanganeh, S. H., Chapi, K., Singh, V. P., Shirzadi, A., Shahabi, H., & Pham, B. T. (2019). Mapping groundwater potential using a novel hybrid intelligence approach (Random Subspace–Random Forest). *Water Resources Management*, *33*(1), 281–302. https://doi.org/10.1007/s11269-018-2102-6

Morgan, H., Madani, A., Hussien, H. M., & Nassar, T. (2023). Using an ensemble machine learning model to delineate groundwater potential zones in desert fringes of Upper Egypt. *Geoscience Letters*, *10*(1), 9. https://doi.org/10.1186/s40562-023-00261-2

Naghibi, S. A., Moghaddam, D. D., Kalantar, B., Pradhan, B., & Kisi, O. (2017). Comparative assessment of GIS-based data mining models and a novel ensemble model in groundwater well potential mapping. *Journal of Hydrology*, *548*, 471–483. https://doi.org/10.1016/j.jhydrol.2017.03.020

Naghibi, S. A., Dolatkordestani, M., Rezaei, A., Kalantar, B., & Pradhan, B. (2019). Application of rotation forest with decision trees as base classifiers and a novel ensemble model in groundwater potential mapping. *Environmental Monitoring and Assessment*, *191*(4), 129. https://doi.org/10.1007/s10661-019-7362-y

Naghibi, S. A., Hashemi, H., Berndtsson, R., & Lee, S. (2020). Application of extreme gradient boosting and parallel random forest algorithms for assessing groundwater spring potential using DEM-derived factors. *Journal of Hydrology*, *589*, 125197. https://doi.org/10.1016/j.jhydrol.2020.125197

Nesmeyanov, S., Umurzakov, R., Rabbimkulov, S., & Voeykova, O. (2021). Determination of structural-geomorphological and

neotectonic elements controlling the oil and gas performance of the Ferghana region using digital space images. *Technical Science and Innovation*, *2021*(1), 130–140. https://doi.org/10.51346/tstu-01.21.1-77-0101
Oh, H. J., Kim, Y. S., Choi, J. K., Park, E., & Lee, S. (2011). GIS mapping of regional probabilistic groundwater potential in the area of Pohang City, Korea. *Journal of Hydrology*, *399*(3–4), 158–172. https://doi.org/10.1016/j.jhydrol.2010.12.027
Panahi, M., Sadhasivam, N., Pourghasemi, H. R., Rezaie, F., & Lee, S. (2020). Spatial prediction of groundwater potential mapping based on convolutional neural network (CNN) and support vector regression (SVR). *Journal of Hydrology*, *588*, 125033. https://doi.org/10.1016/j.jhydrol.2020.125033
Paul, R. S., Rawat, U., SenGupta, D., Biswas, A., Tripathi, S., & Ghosh, P. (2020). Assessment of groundwater potential zones using multi-criteria evaluation technique of Paisuni River Basin from the combined state of Uttar Pradesh and Madhya Pradesh, India. *Environmental Earth Sciences*, *79*(13), 340. https://doi.org/10.1007/s12665-020-09091-3
Rahmati, O., Pourghasemi, H. R., & Melesse, A. M. (2016). Application of GIS-based random forest and maximum entropy models for groundwater potential mapping: A case study in Iran. *Catena*, *137*, 360–372. https://doi.org/10.1016/j.catena.2015.10.010
Rasool, U., Yin, X., Xu, Z., Rasool, M. A., Senapathi, V., Hussain, M., & Trabucco, J. C. (2022). Mapping of groundwater productivity potential with machine learning algorithms: A case study in Quetta, Pakistan. *Chemosphere*, *303*, 135265. https://doi.org/10.1016/j.chemosphere.2022.135265
Razandi, Y., Pourghasemi, H. R., Neisani, N. S., & Rahmati, O. (2015). Application of AHP, frequency ratio and certainty factor models for groundwater potential mapping using GIS. *Earth Science Informatics*, *8*(4), 867–883. https://doi.org/10.1007/s12145-015-0220-8
Rizeei, H. M., Pradhan, B., Saharkhiz, M. A., & Lee, S. (2019). Groundwater aquifer potential modeling using an ensemble multi-adoptive boosting logistic regression technique. *Journal of Hydrology*, *579*, 124172. https://doi.org/10.1016/j.jhydrol.2019.124172
Roy, A., Naikoo, M. W., Rahman, A., & Sobnam, M. (2022). Novel hybrid models to enhance the efficiency of groundwater potentiality mapping. *Applied Water Science*, *12*(4), 102. https://doi.org/10.1007/s13201-022-01571-0
Zhang, J., Zhou, X., & Long, H. (2020). Late Quaternary loess accumulation at the Rudak section in Uzbekistan, Central Asia: Chronology and palaeoclimate implications. *Palaeogeography Palaeoclimatology Palaeoecology*, *547*, 109695. https://doi.org/10.1016/j.palaeo.2020.109695